

# Multipurpose experimental characterization of smart nanocomposite cement-based materials for thermal-energy efficiency and strain-sensing capability

Anna Laura Pisello<sup>a,b,\*</sup>, Antonella D'Alessandro<sup>c</sup>, Sara Sambuco<sup>a,b</sup>, Marco Rallini<sup>c</sup>, Filippo Ubertini<sup>a,c</sup>,  
Francesco Asdrubali<sup>a,d</sup>, Annibale Luigi Materazzi<sup>c</sup>, Franco Cotana<sup>a,b</sup>

<sup>a</sup>CIRIAF-Interuniversity Research Center, Engineering Department, Via G.Duranti, Perugia, Italy

<sup>b</sup> Department of engineering, University of Perugia, via G. Duranti, 06125 Perugia, Italy

<sup>c</sup> Department of Civil and Environmental Engineering, University of Perugia, via G. Duranti3, 06125 Perugia, Italy

<sup>d</sup> Department of Engineering, University of "RomaTre", via Vito Volterra 62, Roma 00146, Italy

## ABSTRACT

Novel nanocomposite smart multifunctional materials are emerging as promising technological advances in construction industry, where thermal-energy efficiency needs should meet environmental sustainability and mechanical performance requirements. In this view, new cement-based materials showed encouraging results in terms of added functional properties combining all the above mentioned capabilities with electrical conductivity and self-sensing potential for a variety of field scopes, e.g. vibration measurements, damage detection, structural health monitoring, electromagnetic shielding, self-heating pavements for deicing and more.

The present paper deals with the development and multipurpose experimental characterization of cement-based materials doped with different carbon nanoinclusions consisting of: multi-walled carbon nanotubes, carbon nanofibers, carbon black, and graphene nanoplatelets. The study investigates morphology, optical features, thermal characteristics, electrical properties and strain-sensing capability of the different composites, through a campaign of in-lab experimental measurements. The results highlight the peculiar behavior of each composite material, which is strictly related to the adopted nanoinclusions, that reveal to be suitable for specific purposes. In particular, all carbon nanoinclusions are seen to reduce solar reflectance

capability, while they produce negligible variations in thermal emittance. Graphene nanoplatelets represent the most effective nanoinclusion to increase thermal conductivity and diffusivity, which is related to their structural and geometrical characteristics and better capability to distribute the thermal wave. Consistently, the same graphene samples produce the largest electrical conductivity and capacitance. However, multi-walled carbon nanotubes, even though providing comparatively smaller contributions to electrical conductivity, are seen to be the best nanoinclusions for providing strain-sensing capabilities to the cement-based composites.

**Keywords:** smart multifunctional cement-based composites, cement-based materials, nanotechnology, thermal-energy efficiency in buildings, self-sensing materials, cement-based sensors.

## 1. Introduction

High environmental performance and smart materials are achieving increasing attention from the scientific community and the industrial one for their promising multifunctional behavior and their beneficial potentialities such as key environmental performance, promising energy efficiency optimization, high structural strength, enhanced durability and new construction technologies [1-2]. In this view, starting from the first structural development toward high strength concrete [3-4], innovative multifunctional cement-based materials are under development and testing with the final aim to optimize their further potentialities, by paying dedicated attention to their environmental sustainability behavior [5-6] and to the role that nanostructured particles play on such properties [7]. Among other applications, the analysis and the optimization of optic-energy and thermal properties of such cement-based media captured the attention of researchers aimed at optimizing thermal-energy performance in buildings and outdoor thermal comfort conditions [8-9]. Additionally, further potentialities of such materials, such as their electrical features for strain-sensing applications in constructions enabling direct crack detection capabilities and providing distributed strain data for Structural Health Monitoring (SHM), are currently under fast progress [10].

Within the wide and sprawling variety of new smart materials for building thermal-energy efficiency, carbon-based nano-additives for inclusion in cement-based materials certainly showed highly promising features with multipurpose optimization potential. Starting from this acknowledgment, this research paper is aimed at presenting a multipurpose study dealing with the experimental characterization of cement-based

materials doped with different carbon nanoinclusions, by taking into account their (i) morphological and nanostructural characteristics, (ii) thermal-energy and optical features, (iii) mechanical behavior, (iv) electrical properties and (v) piezoresistive strain-sensing potential, with the final purpose to provide an exhaustive panorama around the potential applications of such innovative solutions for smart and multifunctional cutting edge constructions. To this aim, the present work presents the key research background in the field (Section 2), the considered materials and the acknowledged methodologies for their multipurpose characterization by means of multidisciplinary experimental procedures (Section 3). Then, the final discussion around the main achieved results is dealt with in Section 4, and the key conclusions are reported in the final Section 5.

## **2. Research background**

The present work builds upon previous contributions mainly focused on the development and multipurpose characterization of innovative materials for building thermal-energy efficiency [11-12] by means of passive strategies such as materials with passive cooling potential [13], materials with sensible or latent heat storage capability [14-15], or other bioinspired systems incorporated into building envelope [16-17]. In this perspective, cement-based materials are preparing a breeding ground for interesting research development, given the huge diffusion and tradition of such materials for both structural and architectural purposes. About their optimization for building thermal-energy efficiency, one of the most investigated areas consisted of the inclusion of thermal storage particles such as phase change materials (PCMs) into the cement medium, in order to optimize its latent thermal storage capability, producing key benefits in stabilizing indoor temperature and also reducing building indoor overheating in summer [18]. In this area, many researches were carried out in the last few decades demonstrating the effect of microencapsulated PCMs into cement media, as it was reported in the review by Khudhair and Farid [19]. Another relevant issue that was addressed in the research on cement-based materials concerned the analysis of their environmental performance in terms of carbon footprint and embodied energy [20], aimed at minimizing the overexploitation of natural resources and raw materials in the construction sector, and also its effect on urban dense microclimate conditions [21]. Another study [22] about the same issue showed that the production and use of cement-based materials deserve to be environmentally optimized, given that they are not yet sustainable being cement production the highest contributor in terms of primary energy demand for the manufacture of 1 m<sup>2</sup> of gross floor area after the only steel and ceramic material. Also, it was considered as the main responsible manufacture process of the CO<sub>2</sub> emissions for the construction of 1 m<sup>2</sup> of gross floor area [23]. In this view, the research around this material was directed towards (i)

minimizing its environmental impact and (ii) investigating innovative and promising cutting edge nanotechnology potentialities, that could motivate the use of such energy needy material, even in the view of a more sustainable construction industry.

The latter aforementioned research topic marked the path to the analysis of high performance concrete achieved by means of silica nanoparticles, silica fume, fly ash [24], and other carbon-based nanoparticles such as those investigated in this work, i.e. carbon nanotubes and nanofibers, carbon black, and graphene nanoplatelets [25-27]. Carbon nanotubes received much attention and gained important success given their capability to make the cement-based material behaving as a piezoresistive medium, with key strain-sensing functional properties having multiple potential applications in smart constructions [10, 28-30]. More in particular, smart piezoresistive cement-based materials doped with conductive nanoinclusions have the potential to provide any concrete structure with self-sensing capabilities by correlating the change of strain with the change of proper electrical properties, such as resistance or conductivity [31-34]. Several factors may affect the electrical characteristics' of the composites: the intrinsic resistance of functional fillers, the bonding between functional fillers and matrix, the contact between functional fillers, the tunneling distance between functional fillers and their electrical capacitance [35]. The presented materials with conductive fillers permitted the fabrication of sensors with enhanced properties in comparison to off-the-shelf sensors: higher durability, the possibility to provide distributed strain data and the consequent potential for effectively scaling the principle of SHM to the case of large-scale structures.

Possible applications of nano-modified cement-based materials were showed to be multidisciplinary and to pertain to the fields of SHM, construction industry, smart structures and smart cities [36-39]. Owing to their large and multidisciplinary innovation potential, the scientific literature shows a growing interest in the study of these multifunctional materials. However, much research work still needs to be done concerning prerogatives and issues related to composites' production, performance and modeling [40-42].

Framing into the panorama presented above, this work aims to contribute to a more aware understanding of the multifunctional properties of emerging cement-based materials doped with different carbon nanoinclusions, with a focus on the effects of such additives in modifying the thermal-energy and optic properties of the composites that have been rarely investigated in the literature. In particular, feeling that multiperspective analysis of such materials deserves further research attention as recently dedicated by the scientific community, a multipurpose experimental characterization of cement paste samples doped with multi-walled carbon nanotubes, carbon nanofibers, carbon black and graphene nanoplatelets, is presented,

investigating these composites from multiple perspectives, including (i) thermal-energy and optic characteristics, as well as (ii) electrical and piezoresistive behavior for strain-sensing purpose and mechanical properties.

### **3. Materials and methods**

#### 3.1 Description of the materials

The samples prepared for the experimental campaign were made of cement paste doped with carbon-based conductive nanoinclusions. Four different nanofillers were used: Multi-walled Carbon Nanotubes (MWCNTs), Carbon Nano-Fibers (CNFs), Carbon Black (CB) and Graphene NanoPlatelets (GNPs).

The MWCNTs chosen for the samples were Arkema Graphistrength C100. They belong to the structural family of Fullerene and they consist of multiple concentric rolled graphene sheets. Carbon atoms are arranged in a hexagonal pattern with strong covalent bonds, type  $\sigma$ - $\sigma$ , while the tubes are connected through Van der Waals forces. Such attractive forces determine the development of bundles, undesirable structures that complicate the task of achieving a homogeneous material [43-45]. MWCNTs have a macroscopic appearance as black powder, with a very high specific surface area (of the order of 100-250 m<sup>2</sup>/g) and very low apparent density (of the order of 50-150 kg/m<sup>3</sup>) [46-48].

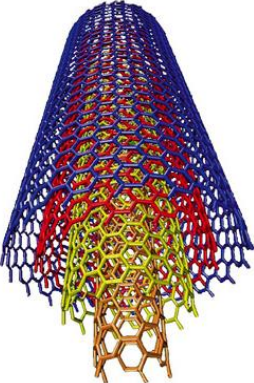

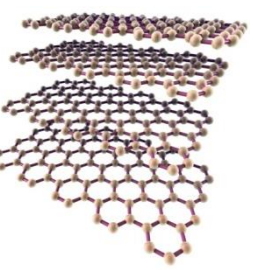

The Carbon Nanofibers used for preparing the cement paste specimens, type Pyrograf-III Carbon Nanofiber PE-19-XT-LHT, had a unique stacked-cup structure consisting of graphene plane surfaces canted from the fiber axis. They were produced by a low heat treatment with temperatures up to 1500°C, which partially chemically graphitized the vapor deposited carbon on the surface and allowed to obtain ordered structures, with diameters ranging from 70 to 200 nm and lengths between 50 and 200 microns.

The Carbon Black fillers chosen for the research experimentation were provided by Orion Printex XE-2B. They were composed of pure elemental carbon, in the form of colloidal spherical particles, produced by the incomplete combustion of organic materials such as petroleum or coal. Carbon black pigments are capable to impart electrical conductivity both in water and solvent borne systems. Electron tunneling is one of the factors influencing the electrical conductivity of such nanoparticles, property which comes from the capacity of electrons to jump the gaps between the closed carbon black aggregates [49].

The Graphene Nanoplatelets, produced by Cheap Tubes Inc., were chemically exfoliated from natural graphite. They consisted of small stacks of graphene with an overall thickness of approximately 3-10 nm. The nanoplatelets are excellent electrical and thermal conductors as a result of their pure graphitic composition. Unlike the other nanofillers used in the research, they are two-dimensional, resulting in the achievement of isotropic nanomodified composites [50].

Table 1 summarizes the main physical, chemical and mechanical properties of all the nanofillers adopted in this paper.

**Table 1.** Properties of nanofillers used in the experimentation

Nanofiller	Properties		Nanofiller	Properties	
<b>MWCNTs</b>	Outer mean diameter	10 – 15 nm	<b>Carbon Nanofibers</b>	Fiber diameter (average)	150 nm
	Mean agglomerate size	200-500 $\mu\text{m}$		CVD carbon overcoat on fiber	no
	Weight loss at 105 °C	<1%		Surface area	20-30 $\text{m}^2/\text{g}$
	C content	> 90 wt%		Dispersive surface energy,:	120-140 $\text{mJ}/\text{m}^2$
	Free amorphous carbon	Not detectable SEM/TEM		Polyaromatic hydrocarbons:	<1 mg PAH/gmfiber
	Mean number of walls	5 – 15		Iron	<14,000 ppm
	Apparent density	50 – 150 $\text{kg}/\text{m}^3$		Density	1.0 $\text{g}/\text{cm}^3$
	Length	0.1 – 10 $\mu\text{m}$		Moisture	<5 wt%
<b>Graphene Nano Platelets</b>	Diameter (average)	15 $\mu\text{m}$	<b>Carbon Black</b>	Particle Size (average):	30 nm
	Purity	97 wt %		Blackness Value M	216
	Grade	2		Oil Absorption Number (OAN)	420
	Surface Area	100 $\text{m}^2/\text{g}$		Volatile (950°C)	-
	Density	1.8 $\text{g}/\text{cm}^3$		Density	1.8 $\text{g}/\text{cm}^3$

The samples were prepared by following the mix design reported in Tab. 2. The cement pastes consisted of a mixture of Portland cement type 42.5 with a water/cement ratio of 0.4. The nanofillers were added in the amount of 2% by mass of cement. A plasticizer based on second-generation polycarboxylate ether polymers was added to the mix in variable amounts to increase workability and to improve the dispersion of the

nanoinclusions in the matrices. In particular, 1% of plasticizer by mass of cement was used for the specimens with MWCNTs and CB, and 1.5% for samples with CNFs and GNPs. The samples were in the form of prisms of dimension  $40 \times 40 \times 160 \text{ mm}^3$ . No aggregates were included in the mix design. This was motivated by the circumstance that the cement paste is more homogeneous if compared to mortar and concrete and allows to better highlight the contributions of the nanofillers to the investigated properties of the composites.

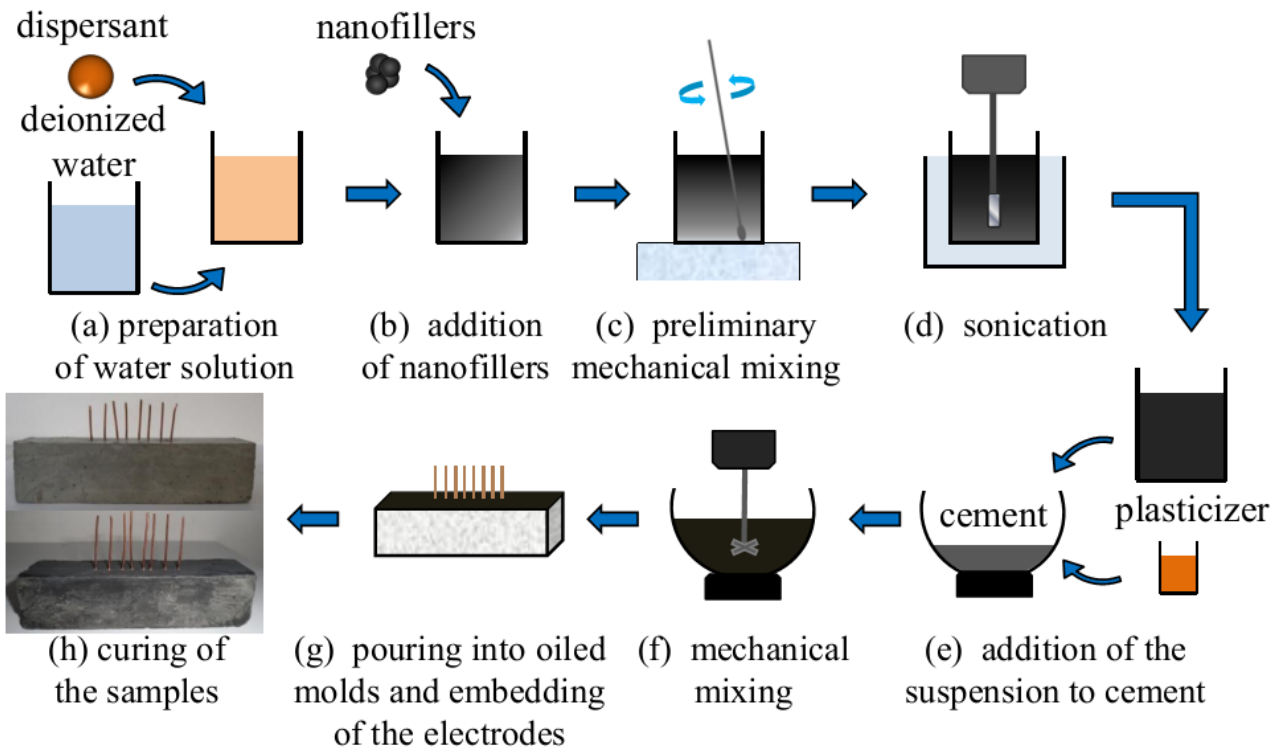
**Table 2.** Mix design of nanomodified cement pastes

<b>Components</b>	<b>kg/m<sup>3</sup></b>	<b>g/sample</b>
Nanoinclusions	32.4	8.3
Portland Cement 42.5 R	1620	415
Polycarboxylate ether-based Plasticizer	var.	var.
Water	665	166
w / c ratio	0.4	0.4

Due to their morphology and dimension, the dispersion of carbon nanofillers in an aqueous solution, to achieve prior to the addition of cement powder to obtain the paste, is a rather delicate task, because the nanoparticles tend to agglomerate in bundles. In order to prepare a cementitious nanomodified material that is as much homogeneous as possible, the fabricating process was divided into two steps. Firstly, a solution of deionized water and plasticizer, used as a dispersant, was created (Fig. 1(a)), and the nanofillers were dispersed in the water solution with a preliminary mechanical mixing (Fig. 1(c)) and 30 minutes of sonication at 225 W (Fig. 1(d)). Secondly, the water suspension and the plasticizer were added to cement powder (Fig. 1(e)). Then, the dough was mechanically mixed (Fig. 1(f)), poured into oiled molds and then the electrodes were embedded (Fig. 1(g)). After solidification, the samples were unmolded for curing in laboratory controlled conditions (Fig. 2(h)). Fig. 1 illustrates the step-by-step fabricating process.

In the following experiments, the reference, plain, cement paste is indicated as "PASTE 0", while composite paste specimens with MWCNTs, CNFs, CB and GNPs are indicated as "PASTE CNT" (MWCNT are briefly indicated as CNT), "PASTE CNF", "PASTE CB" and "PASTE GNP", respectively. For spectrophotometric measurements, a reference concrete sample is also considered, in order to show the difference between a classic concrete and a classic paste with no inclusions.

-----



**Figure 1.** Fabricating process of nanomodified cement paste samples.

The ultrasound device used in the sonication was a Vibra Cell Bioblock Scientific, model 75043. During sonication, the water suspensions were covered by an aluminum sheet and were kept immersed in a cold bath, in order to limit evaporation. The electrodes were eight 1 mm-diameter copper wires. They were inserted by approximately the 85% of the thickness of the specimens, in the centre of the samples and placed symmetrically along the central axis. The internal ones were placed at a distance of 1 cm, while the external ones at a distance of 6 cm. The use of wire electrodes, instead of bidimensional nets as used in other studies by the authors [10,25,36,40], which resulted in a local electromechanical investigation of the composites, was motivated by the need of reducing as much as possible the effects of the electrodes on the thermal properties of the samples.

### 3.2 Experimental procedure to test inner thermal characteristics

Measurements of thermal conductivity and thermal diffusivity were performed with the Hot Disk Thermal Constants Analyser manufactured by Hot Disk. Hot disk method is based on the theory of the Transient Plane Source (TPS) technique (recognized in ISO 22007 - 2 [32]) and consists of the use of a



transiently heated plane sensor characterized by an electrically conducting pattern in the shape of a double spiral etched out of a thin sheet of Nickel. The spirals are sandwiched between two thin layers of Kapton, an electrically insulating material. The sensor is fitted between two pieces of sample, each one with a plane surface facing the sensor. It acts both as a heat source for increasing the temperature of the sample and as a resistance thermometer for recording time-dependent temperature increase.

Several methods are commonly used to measure the thermal conductivity and it is possible to subdivide them in two main categories: steady-state and non-steady-state (transient) methods. In the former methods, specimens are put in contact with a heat source and with temperature sensors, and the equilibrium is reached at a given temperature. In the latter methods, a thermal transient is produced by a heat pulse to generate a dynamic temperature field within the specimen [51-52]. Steady-state heat transfer properties can be measured for example by the guarded hot plate and the heat flow technique, but there are a number of standardized test methods [51]. Thermal properties by transient method may be determined by hot wire, pulse transient and plane source transient. The advantages in using hot disk are the possibility to make measurements on samples of materials of limited size and the possibility to measure both thermal conductivity and thermal diffusivity [52]. The form of the plane surface may be arbitrary as long as the distance from the hot disk to the nearest sample boundaries is larger than the probing depth  $\Delta p$  defined as:

$$\Delta p = 2 \sqrt{\kappa \cdot t}$$

where  $\kappa$  is the thermal diffusivity of the sample,  $t$  is the measuring time of the experiment and the constant 2 was determined to minimize the influence of external sample boundaries [53-54]. The behavior of the hot disk is described by assuming that the heat source is located in an infinitely large sample. The time dependent thermal resistance increase is expressed by the following relation [52]:

$$R(t) = R_{t=0} \{1 + \alpha [\Delta T_i + \Delta T_s(\tau)]\}$$

where  $R_{t=0}$  is the resistance of the disk just before heating or at a time  $t = 0$ ,  $\alpha$  is the temperature coefficient of the thermal resistance,  $\Delta T_i$  is the increase in temperature over the insulating layers of the probe while  $\Delta T_s(\tau)$  is the increase in the temperature of the specimen surface defined as:

$$\Delta T_s(\tau) = P_0 (\pi^{3/2} r \lambda)^{-1} D(\tau)$$

where  $P_0$  is the power output from the sensor,  $r$  is the overall radius of the disk,  $\lambda$  is the thermal conductivity of the specimen material and  $D(\tau)$  is the dimensionless specific time function with

$$\tau = \sqrt{\frac{t}{\theta}}$$

where  $t$  is measured from the transient beginning and  $\theta$  is the characteristic time defined as:

$$\theta = \frac{r^2}{\kappa}$$

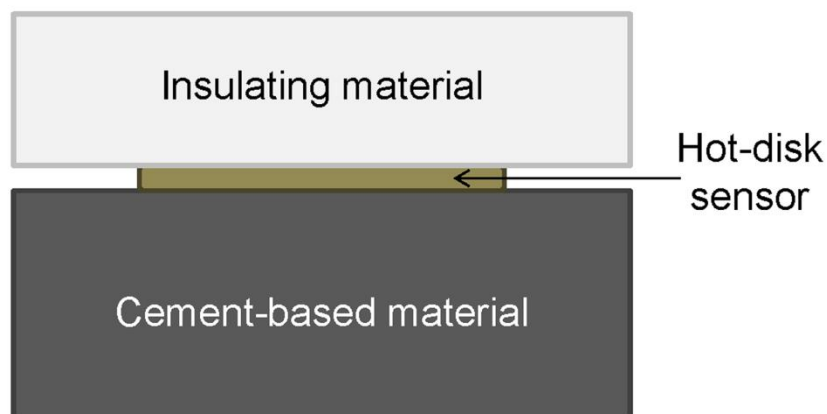
By making a plot of the measured resistivity  $R(t)$  versus  $D(\tau)$ , it is possible to get a straight line from which the thermal conductivity is obtained through a process of iteration. Therefore, the thermal conductivity and the thermal diffusivity are determined from one single transient recording. The relation between thermal conductivity and thermal diffusivity of the sample material is:

$$\lambda = \rho C_p \kappa$$

where  $\rho$  is the density of the sample and  $C_p$  is the specific heat of the sample.

The parameters used to perform the measurements of thermal conductivities from 0.005 W/mK to 1800 W/mK are the (i) heating power to increase the temperature of the spiral, (ii) the measurement time for recording 200 points and (iii) the size of the sensor.

The experimental measurements carried out in this work refer to the option called “single sided experiment” [54] where the sensor is fitted with an insulating material on one side and the sample on the other (Fig. 2). The reference insulating material is a polystyrene with thermal conductivity of 36 mW/mK and thermal diffusivity of  $690e^{-3} \text{ mm}^2/\text{s}$ .



**Figure 2.** Sketch of the setup and photography of the thermal conductivity and thermal diffusivity measurements on nanocomposite cement-based specimens by Hot Disk method.

For each sample, 18 measurements were carried out in 6 different surface points by taking into consideration the heterogeneity of the material under examination. As shown in Tab. 3, the waiting time between each measurement was 1800 s in order to dissipate the imposed thermal pulse. The radius of the sensor was 6.403 mm, and the heating power depended on the sample type, while the measurement time was 40 s. The room temperature was controlled and kept constant at 19°C.

**Table 3.** Samples and tests characteristics

	Size (mm)			Heating Power	Measuring time	Disk Sensor	Room Temperature
	height	width	depth				
<b>PASTE 0</b>	40	40	160	600 mW	40 s	6.403 mm	19°C
<b>PASTE CB</b>	40	40	160	700 mW	40 s	6.403 mm	19°C
<b>PASTE CNT</b>	40	40	160	750 mW	40 s	6.403 mm	19°C
<b>PASTE CNF</b>	40	40	160	750 mW	40 s	6.403 mm	19°C
<b>PASTE GNP</b>	40	40	160	750 mW	40 s	6.403 mm	19°C

After the measurements under normal conditions, the samples were dried to carry out a second stage of measurements. The specimens were placed in a climatic chamber at a temperature of 85°C and relative humidity of 0% for three days. Tab. 4 reports the weight measurements of the dried samples, that were about 10% less than the corresponding ones prior to drying.

**Table 4.** Samples weight values before and after the drying treatment.

	wet	dried
<b>PASTE 0</b>	450 g	415 g
<b>PASTE CNT</b>	461 g	437 g
<b>PASTE CB</b>	460 g	423 g
<b>PASTE CNF</b>	451 g	419 g
<b>PASTE GNP</b>	427 g	395 g

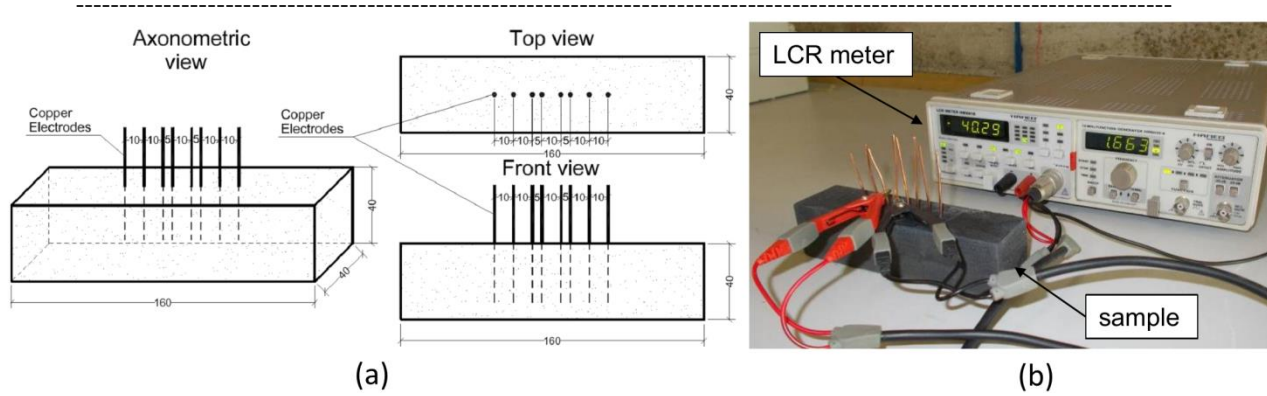
### 3.3 Experimental procedure to test optic-energy characteristics

The analysis of the thermal and optical properties of the cement-based materials was performed by a spectrophotometer for detecting the spectral reflectance of the materials and by a portable thermal emissometer for measuring thermal emissivity of the surfaces. The used spectrophotometer with integrating sphere is a Shimadzu SolidSpec 3700 (Shimadzu Corporation, Kyoto, Japan). Such instrument allowed to take measurements with a spectral bandwidth in the interval  $240 \div 2600$  nm, even if the useful results were considered in the range of  $300 \div 2500$  nm by neglecting the boundaries. The wavelength accuracy corresponded to  $\pm 0.2$  nm in the UV/VIS stripe and  $\pm 0.8$  nm in the NIR interval, while the reading accuracy was  $\pm 2\%$ . The solar hemispherical reflectance of the samples was determined by following the theoretical background described in [55], but without any weighting procedure by means of any reference solar spectrum, in order to detect the specific material variation at each wavelength without any further agent.

The emittance measurements were performed by means of an AE1 RD1 portable emissometer equipped with scaling digital voltmeter. The procedure was developed according to [56]. The experimental apparatus consisted of a differential thermopile radiant energy detector, a heater, a heat sink with a flat surface, two sets of reference standards for the calibration, and the samples to be tested. The cubic samples were also prepared according to the requirements of this test with flat and plain surface where the detector was positioned. The repeatability of  $\pm 0.01$  emittance measurement units had to be considered due to environmental agents affecting the detector response to the radiation heat transfer and its production of a voltage output that is linear with emittance.

### **3.4 Experimental procedure to test electrical properties**

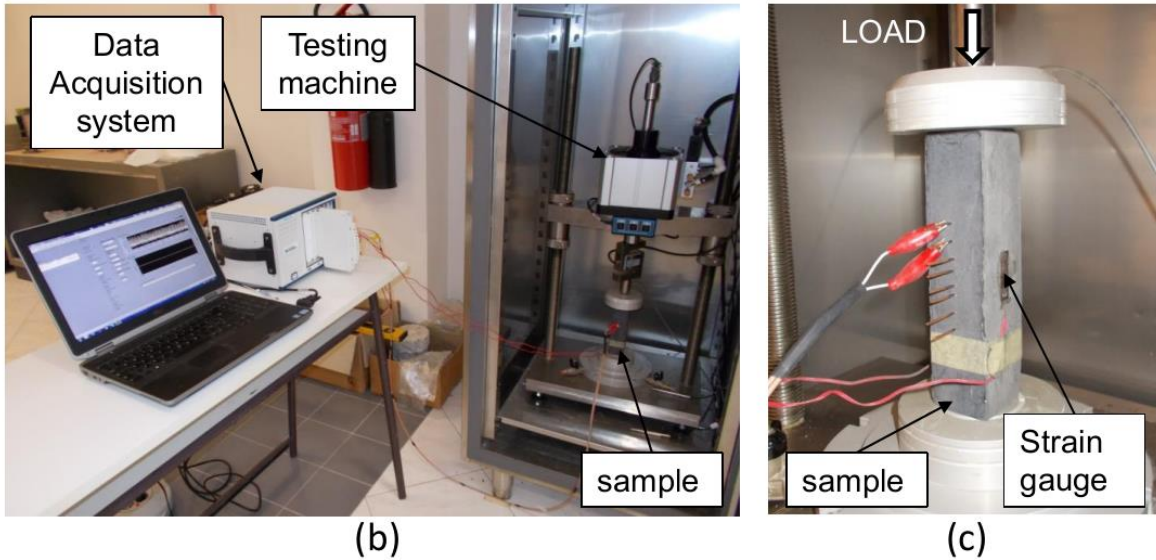
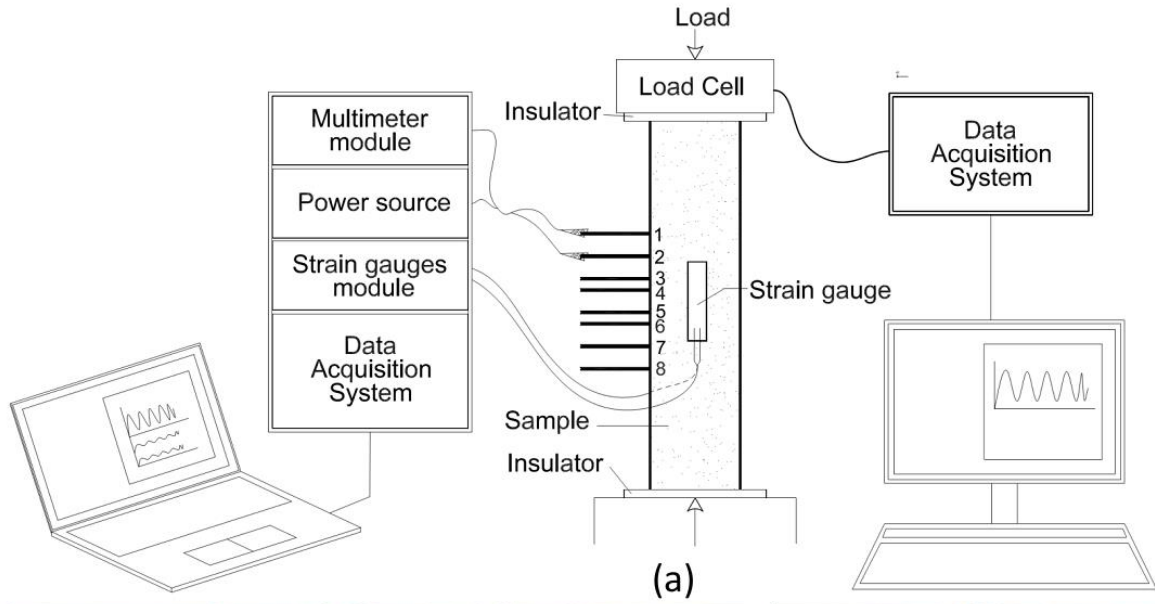
The electrical characterization of the normal and nanomodified cement paste was carried out by using an LCR meter, model HM8018 by Hameg Instruments, using an AC frequency of 25 kHz (Fig. 3). The eight copper wires utilized as electrodes for the electrical tests were positioned as shown in Fig. 3(a). The electrical measurements were carried out using all pairs of electrodes placed at a mutual distance of 10 mm. The LCR meter was used to make AC measurements of electrical resistance and capacitance using different pairs of active electrodes placed at a distance of 1 cm (Fig. 3(b)).



**Figure 3.** Geometry of specimens and positioning of electrodes - dimensions are in mm (a), setup of electrical investigations (b).

### 3.5 Experimental procedure to test the strain-sensing properties

Fig. 4(a) shows the experimental setup of the strain-sensing tests. The sensing specimens (Fig. 4(b)), precompressed at 1 kN, were subjected to harmonically varying axial compression loads, with frequency ranging from 0.1 to 10 Hz. A servo-controlled pneumatic universal testing machine (IPC Global UTM-14P) with 14 kN of load capacity and connected to a data acquisition system was used to apply the time-varying load. The tests were carried out by providing a stabilized voltage input of 6 V to two electrodes placed at a distance of 1 cm (Fig. 4(c)), using a power source unit, model PXI-4130 by National Instruments. The current passing through the specimens was measured by using a high speed digital multimeter, model NI PXI-4071, with a sampling rate of 1000 Hz. Coaxial cables were used to connect the samples to the power source unit and to the multimeter so as to minimize electromagnetic interference. It should be noticed that the applied loads fell within the elastic range of deformation of the cementitious samples and that the investigated frequency range covered the typical range of natural frequencies of civil engineering structures.



**Figure 4.** Setup of electromechanical tests on nanomodified cementitious samples (a), view of the data acquisition system and of the universal testing machine (b), detailed view a sample being tested instrumented with strain gauges and with coaxial cables attached to electrodes (c).

The relationship between the variation of electrical resistance,  $\Delta R$ , normalized to the unstrained resistance,  $R_0$ , and axial strain ( $\epsilon$ ) was modeled in perfectly analogy with electric strain gauges as:

$$\frac{\Delta R}{R_0} = -\lambda \epsilon \quad (1)$$

where  $\lambda$  is the gauge factor of the cement-based sensor. The strain sensitivity,  $S$ , representing the change in electrical resistance per unit change in strain, can be retrieved from (1) and is equal to:

$$S = \frac{\Delta R}{\varepsilon} = -\lambda R_0 \quad (2)$$

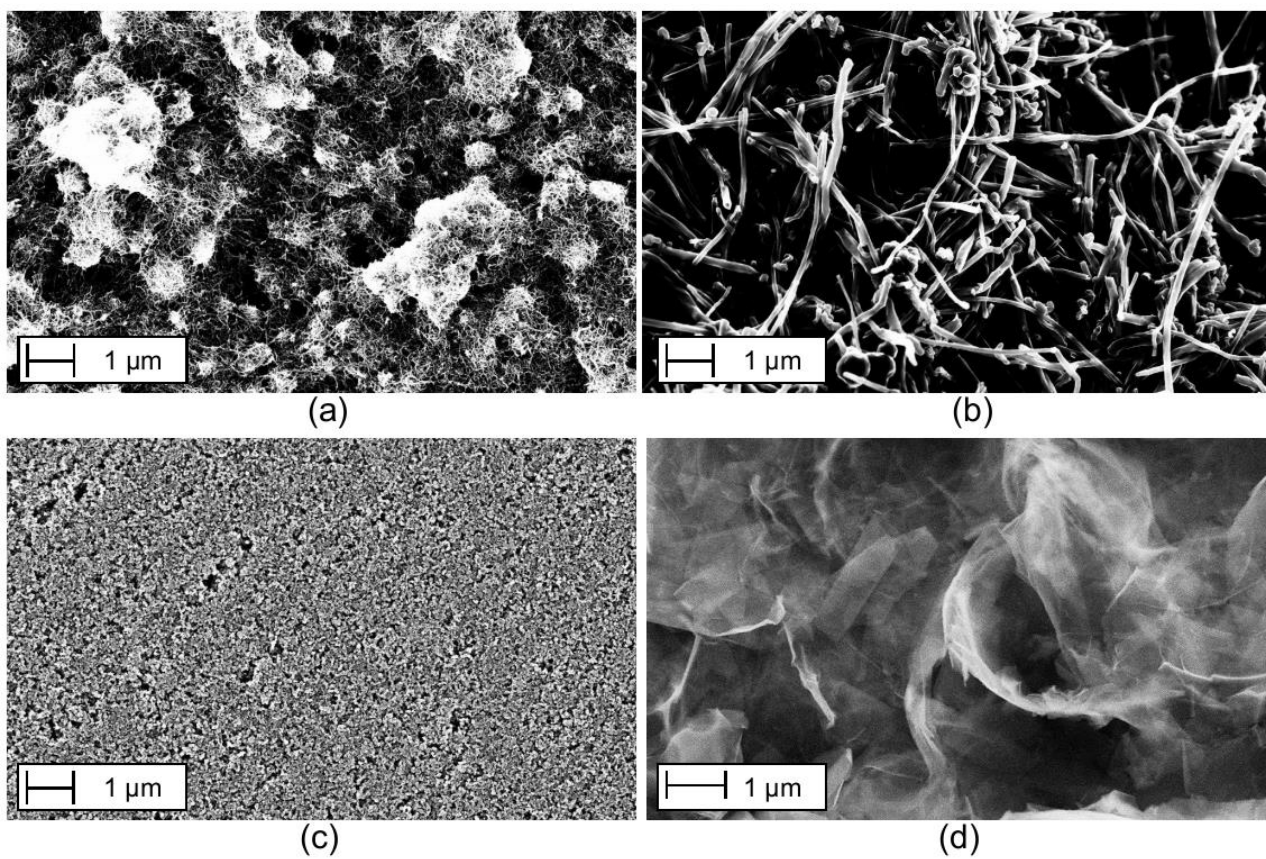
## 4. Results and discussion

### 4.1 Morphological characterization

Figures 5 and 6 show the effective dispersion of the nanofillers into the water solution and in the hardened cement paste, respectively, using a field emission scanning electron microscope (FESEM) ZEISS, model Supra 25. As it concerns the water suspensions, a little drop was poured on a silicon wafer and the water was allowed to evaporate in a spin coater. Instead, for hardened paste, a fragment was directly inserted into the microscope. The micrographs demonstrate a satisfactory dispersion of nanoinclusions in all the admixtures.

Figure 5 highlights the morphological differences of the four nanoinclusions. The four images have the same magnification factor. Multi-walled carbon nanotubes (Fig. 5(a)) and carbon nanofibers have both a predominant-1D structure, but the latter have a larger cross-section (Fig. 5(b)). Carbon black does not exhibit any predominant direction and the particles are randomly distributed (Fig. 5(c)). The graphene nanoplatelets show a predominant-2D structure (Fig. 5(d)). The layers showed to be stacked and connected. The same morphological characteristics are easily identifiable in the SEM micrographs of nanomodified pastes of Fig. 6. The images demonstrate that the mixing method adopted in the experimental campaign did not damage the nanoinclusions. As it concerns the cement paste sample doped with carbon black, an in-lens detector was utilized, in order to obtain an image with high contrast, where single carbon black particles are clearly visible. Due to their morphology, different from other carbon fillers where one or two dimensions appear predominant, CB particles result less recognizable in the cement matrix. However, all the carbon fillers analyzed in the research result acceptably dispersed in the cementitious materials, since particles appear not aggregated in bulky bundles.

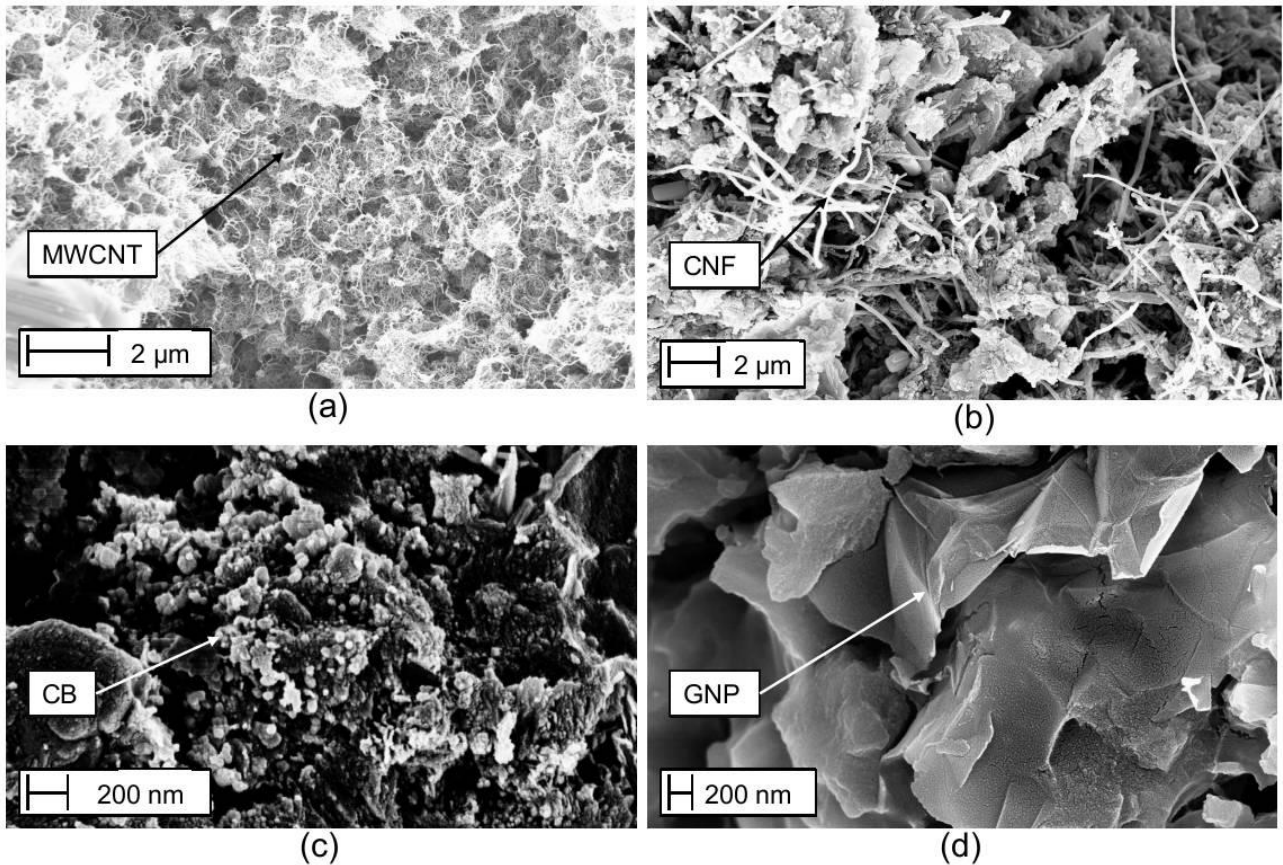
---



**Figure 5.** SEM images of water nanomodified suspensions with MWCNTs (a), CNFs (b), CB (c) and GNPs (d).

---





**Figure 6.** SEM images of nanomodified cement paste with MWCNTs (a), CNFs (b), CB (c) and GNPs (d).

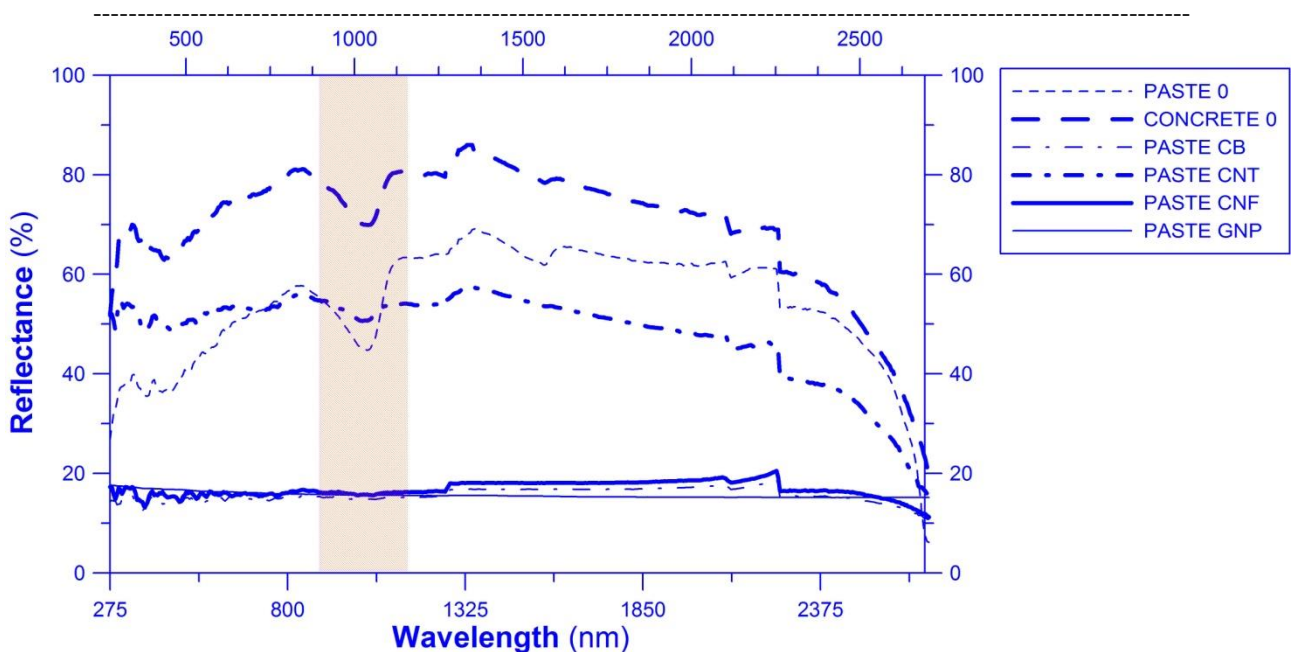
---

#### 4.2 Results of optic-energy characterization of nanocomposite cement-based materials

Fig. 7 reports the spectral solar reflectance of the considered cement-based materials which showed to be largely affected by the nanoparticle inclusion. In particular, the reference concrete sample presents the highest diffused solar reflectance through the overall solar spectrum wavelength interval. Therefore, the corresponding paste with no additives is much more absorptive than the reference concrete, especially in the lower wavelength range. In fact, the PASTE 0 sample consistently shows its reflectance behavior by registering an almost parallel profile with respect to the non-doped CONCRETE 0, that is characteristic of such a material [57] with a closer reflectance behavior in the near infrared region and the characteristic decrease around 1  $\mu\text{m}$ . The nanoadditives in general showed to reduce the spectral variability of the solar reflectance behavior by making the profile flatter and lower in general, with apparent contribution imputable to graphene, carbon fibers and carbon black nanoinclusions. Only graphene shows to interact with the experimental ray at the highest wavelength, conceivably because of the relatively larger size of the nanoparticles, intercepting the near infrared part of the radiation. A singular behavior is instead exhibited by the carbon nanotube filled cement-based

samples which showed interesting potential in increasing their reflectance capability within the ultraviolet range of the test radiation, with promising possible benefits concerning the optimization of their resistance against the damaging UV rays [58], that are responsible of compromising building superficial characteristics and aesthetic features when exposed to solar radiation.

Thermal emittance measurements showed less interesting effects of the considered nanoparticles, demonstrating that they are not able to affect such a superficial property already investigated for cement-based materials. Therefore the positive characteristic of high thermal emittance of concrete based materials is not affected by the studied nanoadditives [58]. In fact, all the samples reported a thermal emittance values around  $0.87 \div 0.90$  without any consistent trend or difference with respect to the reference plain sample.



**Figure 7.** Spectral diffuse reflectance of the tested samples compared to reference concrete and reference PASTE 0 (the shaded area indicates the wavelength range in which cement based materials exhibit the characteristic drop).

### 4.3 Results of thermal characterization of cement-based materials

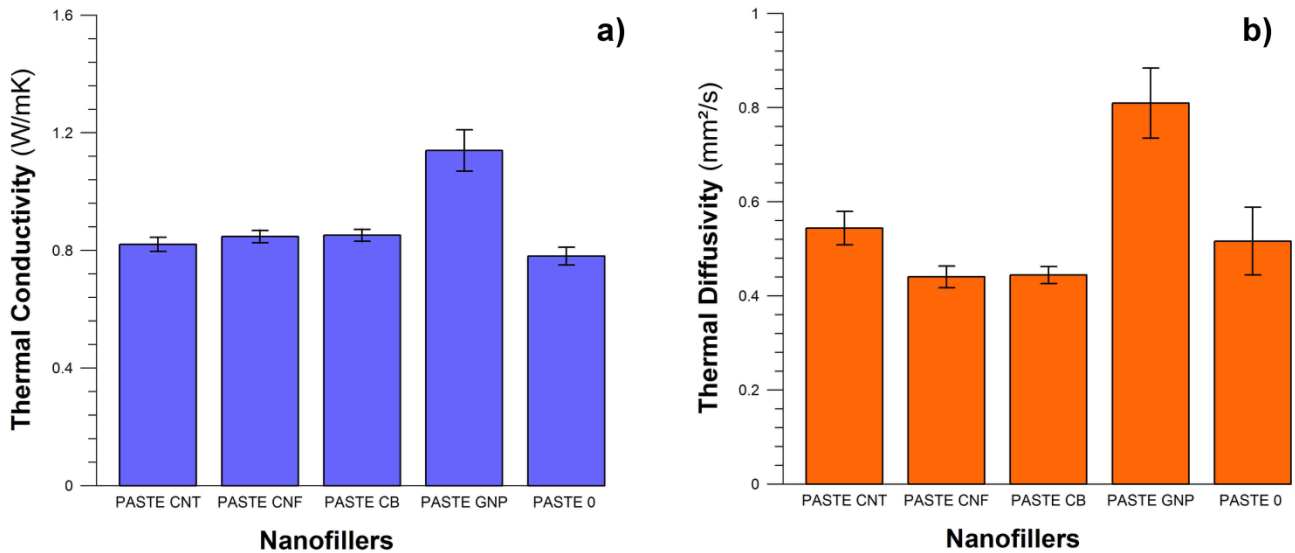
Tab. 5 reports the results obtained by measuring thermal conductivity and thermal diffusivity of the considered cement based materials by the hot disk method.

**Table 5.** Measured thermal conductivity and diffusivity values of the tested samples with plus and minus standard deviation intervals

	<b>Thermal conductivity (W/mK)</b>	<b>Thermal Diffusivity (mm<sup>2</sup>/s)</b>
PASTE-0	0.7804 ± 0.0303	0.5162 ± 0.0720
PASTE-CB	0.8514 ± 0.0200	0.4441 ± 0.0183
PASTE-CNF	0.8469 ± 0.0212	0.4404 ± 0.0232
PASTE-CNT	0.8203 ± 0.0239	0.5438 ± 0.0356
PASTE-GNP	1.1400 ± 0.0702	0.8095 ± 0.0747

Heat insulation or heat conduction enhancement in carbon-based composite materials showed to be influenced by varying the nanoinclusion, consistently with the literature [60] where MWCNTs' orientation demonstrated to affect the thermal performance of the composite material due to the differential interaction among the particles within the network [60]. In fact, previous studies [60] highlighted the impact of geometrical and chemical factors which influence the thermal conductivity in complex networks composed by carbon nanotubes. In particular, aligned MWCNTs can better influence thermal conductivities compared to randomly oriented ones. Comparing the thermal conductivity and thermal diffusivity among the tested samples, the low percentage and the random orientation of nanoparticles in the cement-based matrix are probably the reasons why there is no major increase for Paste CB, CNF, MWCNT with respect to the reference material (Fig. 8). On the other hand, the sample with graphene showed the highest value of conductivity and diffusivity probably imputable to the geometry of nanoparticles (Fig. 6d) allowing a better heat internal conduction and diffusion (Fig. 8). Different values of standard deviation are conceivably imputable to the heterogeneity of the material which is strictly related to the quality of nanoparticles' dispersion.

---

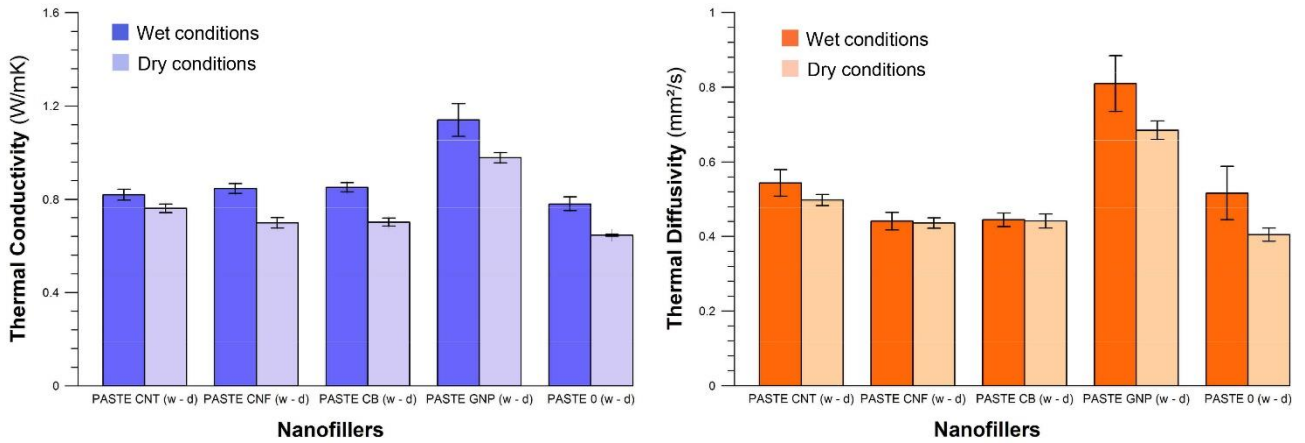


**Figure 8.** Results of measured thermal conductivity (a) and thermal diffusivity (b) by Hot Disk.

Figure 8 also reports the thermal conductivity and the thermal diffusivity of conditioned samples, i.e. in dry and ambient (wet) conditions. The lower content of water is seen to progressively reduce both diffusivity and conductivity, except for the sample with CNTs, which shows a lower relative decrease. The obtained results could depend on a variety of factors [58]. The lower decrease of the thermal conductivity for CNTs can be associated to the higher content of water. This outcome is also consistent with previous studies, as explained, for instance, by Chaban and Prezhdo [60] who demonstrated by molecular dynamics simulation that spatial confinement of water inside carbon nanotubes increases its boiling temperature. For this reason, the drying process had a different effect on the composite paste with MWCNTs in comparison to other specimens that lost more weight.

**Table 6.** Measured thermal conductivity and diffusivity values of the tested dry samples

Thermal conductivity (W/mK)		Thermal Diffusivity (mm <sup>2</sup> /s)	
PASTE 0-d	0,6450 ± 0,0037	PASTE 0-d	0,4045 ± 0,0177
PASTE CB-d	0,7010 ± 0,0176	PASTE CB-d	0,4410 ± 0,0190
PASTE CNF-d	0,6980 ± 0,0223	PASTE CNF-d	0,4353 ± 0,0138
PASTE CNT-d	0,7606 ± 0,0191	PASTE CNT-d	0,4981 ± 0,0146
PASTE GNP-d	0,9782 ± 0,0225	PASTE GNP-d	0,6848 ± 0,0245



**Figure 9.** Results of measured thermal conductivity (a) and thermal diffusivity (b) in dry sample conditions by Hot Disk.

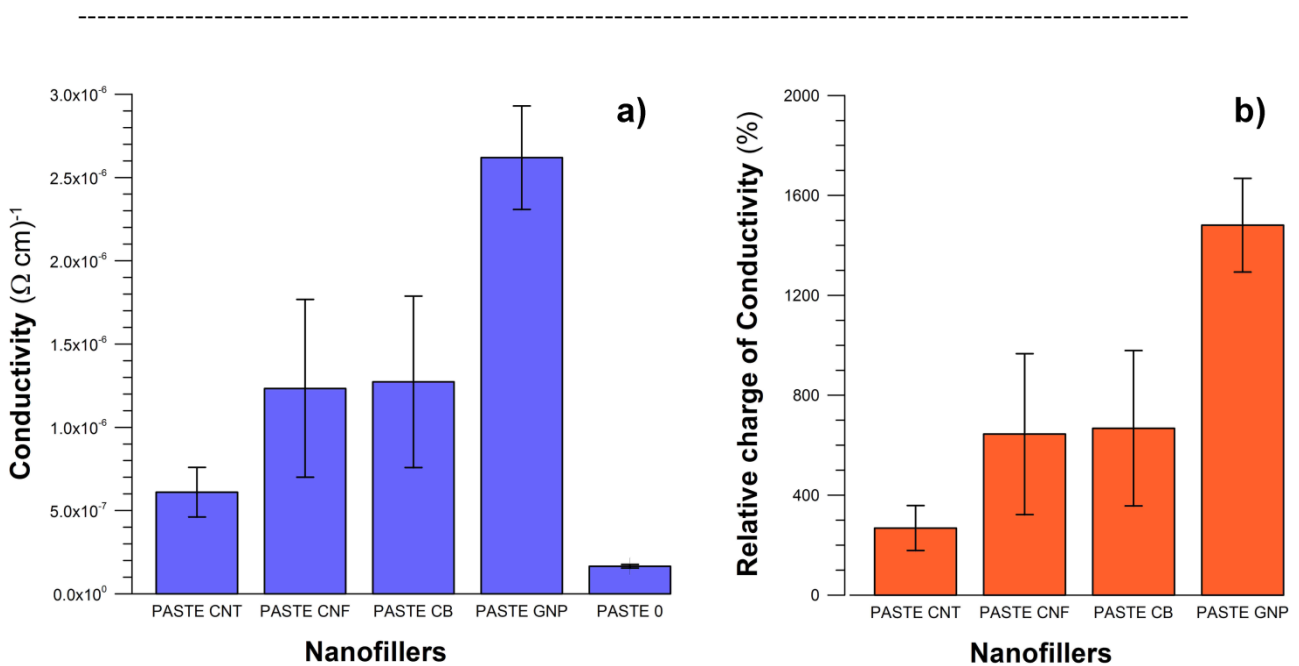
---

#### 4.4 Results of electrical characterization tests

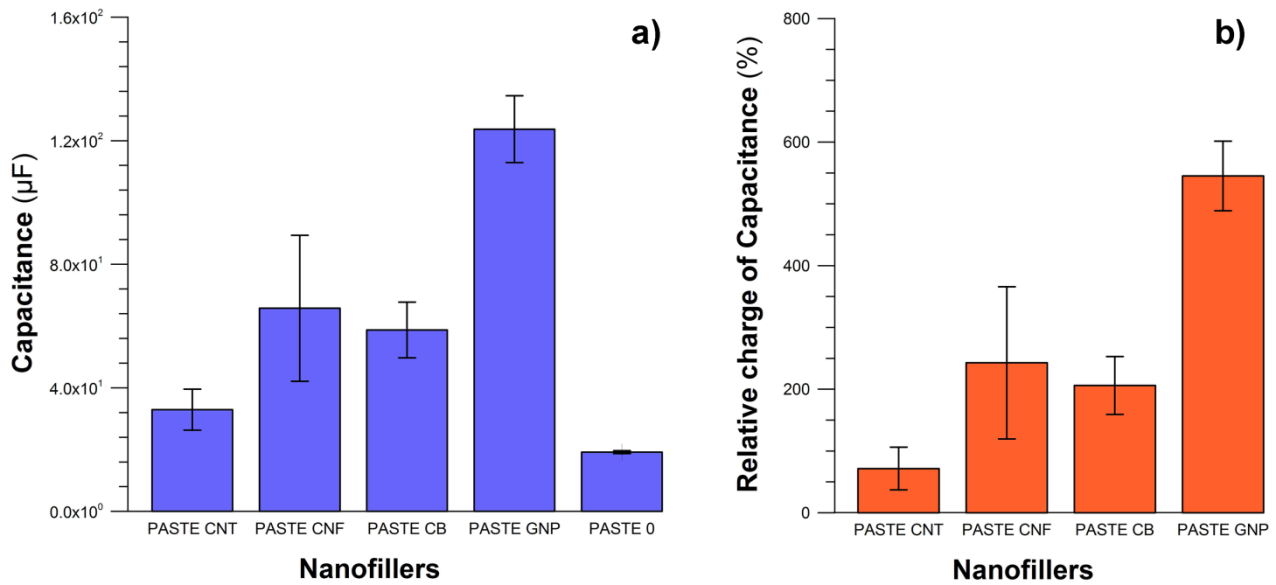
The results obtained from the electrical characterization tests show that the contribution of the nanofillers in increasing the electrical conductivity of the composites is significant. For similar amounts of nanofillers, the largest increase in conductivity is obtained when using GNPs, with a conductivity ranging from  $1.66e-07$  ( $\Omega \text{ cm}$ )<sup>-1</sup> to  $2.62e-06$  ( $\Omega \text{ cm}$ )<sup>-1</sup> for plain and nanocomposite cement paste, respectively. MWCNTs are the nanofillers providing the smallest increase in conductivity, whereby this quantity ranges from  $1.66e-07$  to  $4.54e-07$  ( $\Omega \text{ cm}$ )<sup>-1</sup> for plain and nanocomposite cement paste with nanotubes, respectively. Values of electrical conductivity achieved when using carbon black and carbon nanofibers are very similar ( $8.50e-07$  and  $6.77e-07$  ( $\Omega \text{ cm}$ )<sup>-1</sup>, respectively) and intermediate between composites with MWCNTs and GNPs. Figure 10 shows values of samples' conductivity and their relative change with respect to the plain material, reporting, in both cases, the standard deviation intervals obtained by changing the pairs of active electrodes. Values of electrical capacitance of the samples doped with nanofillers and their relative change with respect to the normal material are reported in Fig. 11. The nanofillers determine increases in electrical capacitance, conceivably because of the interface capacitance between nanofillers and matrix. Electrical capacitance is associated to the extent of polarization and is related to the frequency of the applied current. [61-62]. A similar trend to that of electrical

conductivity is observed, with the largest contribution associated to GNPs and the lowest one to MWCNTs, with similar contributions of CB and CNFs.

Considering that the intrinsic conductivities of the nanofillers are similar in comparison to the much smaller conductivity of the plain cement-matrix material [64-65], the presented results show that the lowest nanoparticle-matrix interface resistance and the highest interface capacitance are obtained with GNPs. This might be associated to a more uniform dispersion of the nanofillers within the matrix and, most of all, to the aspect ratio of the nanofillers, that sensibly reduces from MWCNTs to GNPs. This entails that, in PASTE GNP samples, the same mass quantity of electrically conductive material is subdivided into a smaller number of nanoparticles having larger dimensions with respect to MWCNTs. In particular, the almost bidimensional shape of GNPs seems to enhance interface conduction and capacitance between cement matrix and carbon-based fillers.



**Figure 10.** Electrical Conductivity of normal and nanocomposite samples: absolute values with  $\pm$  standard deviation intervals (a); relative increases in electrical conductivity of nanocomposite materials with respect to plain material (b).



**Figure 11.** Electrical Capacitance of normal and nanocomposite samples: absolute values with  $\pm$  standard deviation intervals (a); relative increases in electrical conductivity of nanocomposite materials with respect to plain material (b).

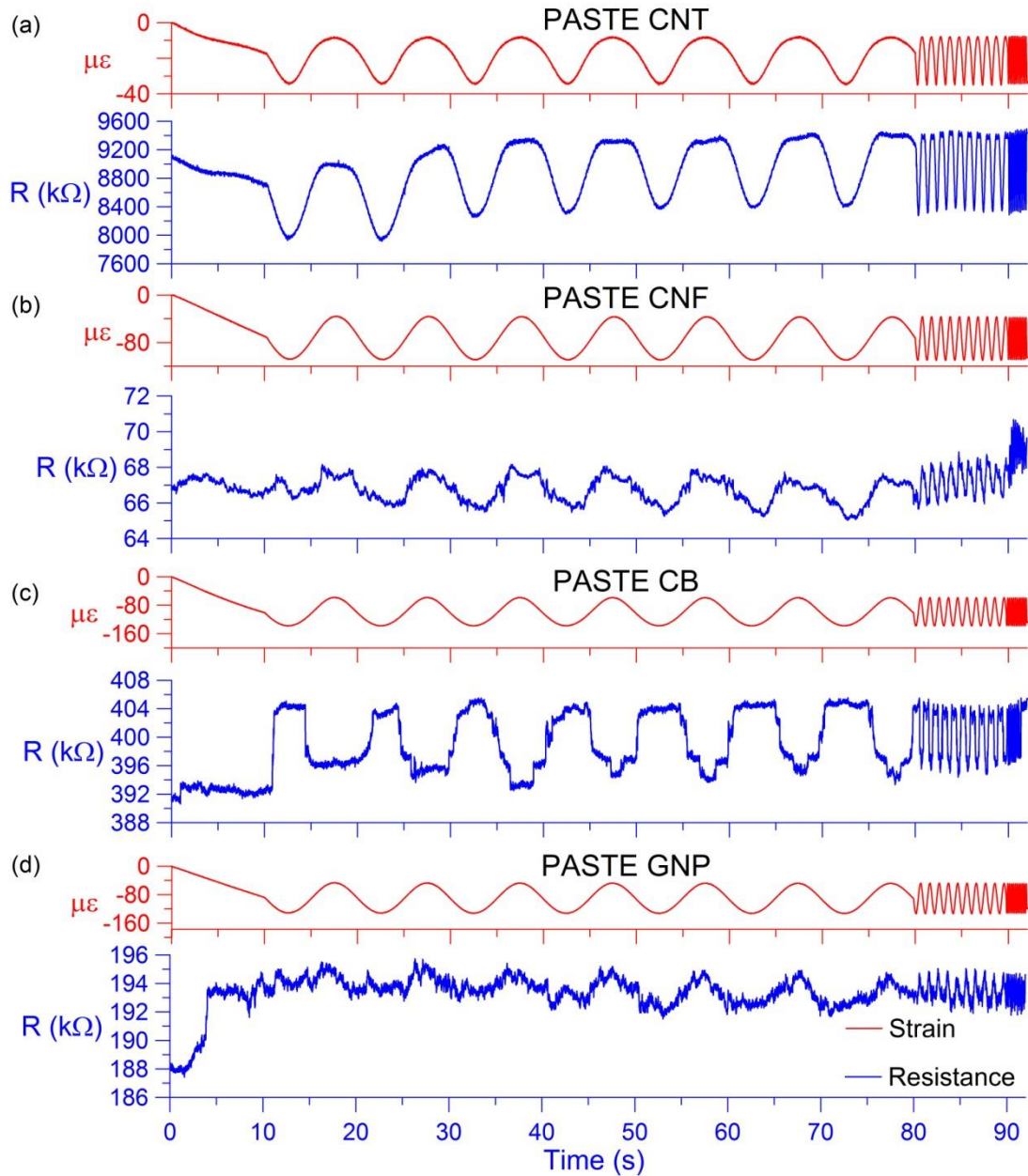
#### 4.4 Results of strain-sensing tests

Fig. 12 shows the responses of the cement-based specimens doped with MWCNTs, CNFs, CB and GNPs, respectively, under application of a harmonic compression load with a frequency ranging from 0.1 to 10 Hz. The figure reports the time histories of the average strain measured with two strain gauges attached on opposite faces of the specimens and the resistance obtained from electrical measurements on the nanomodified specimens. All considered nanocomposite specimens showed a certain sensitivity to strain, although that with MWCNTs exhibited the best quality of the output signal. Plane cement paste does not possess any consistent piezoresistive property and, for this reason, is not included in the figure.

Tab. 7 reports the values of the gauge factor  $\lambda$ , the strain sensitivity  $S$ , defined in Equations 1 and 2, and the Young Modulus  $E$  obtained from the strain-sensing tests. The table also reports information on the unstrained and normalized variation of electrical resistance  $R_0$  and  $\Delta R/R_0$ , respectively, as well as the variation of stress and strain, denoted as  $\Delta\sigma$  and  $\Delta\varepsilon$ , respectively. The results demonstrate the higher gauge factor and strain sensitivity of the sample with MWCNTs, that are both orders of magnitude greater with respect to those obtained using other types of nano-inclusions. It is also worth mentioning that the sample with MWCNTs exhibited the highest Young Modulus,  $E$ , that is, the highest axial stiffness, whereby  $E$  varied from 8821 MPa for the normal cement paste specimen to 23410 MPa for the cement paste specimen doped with MWCNTs.



On the contrary, the Young moduli of specimens doped with CNFs, CB and GNPs were consistently very similar to that of the plane cement paste, which demonstrates the predominant role of the shape and the aspect ratio of the nanoinclusions in determining their effectiveness as mechanical nanoreinforcements.



**Figure 12.** Time histories of measured strain and electrical resistance for samples with MWCNTs, CNFs, CB and GNPs from strain sensing tests.

**Table 7.** Results of strain sensing tests ( $\Delta R/R_0$ ,  $\Delta\epsilon$  and  $\Delta\sigma$  are variations in normalized electrical resistance, axial strain and stress, respectively, under a compression loading cycle ranging from 0.5 to 1.5 MPa;  $R_0$  is the initial resistance,  $\lambda$  is the Gauge Factor,  $S$  the sensitivity and  $E$  the Young Modulus)



Filler	$R_0$ ( $\Omega$ )	$\Delta R/R_0$	$\Delta \epsilon$	$\Delta \sigma$ (MPa)	$\lambda$	S ( $\Omega$ )	E (MPa)
MWCNTs	9.091e6	0.111	2.67e-5	0.625	4139	3.763e10	23410
CNFs	6.678e4	0.041	7.31e-5	0.625	561	3.746e7	8547
CB	3.912e5	0.027	7.94e-5	0.625	340	1.330e8	7875
GNPs	1.881e5	0.020	7.76e-5	0.625	258	4.853e7	8055

## 5. Conclusions

The paper has presented a campaign of experimental tests aimed at investigating morphology, optical features, thermal characteristics, electrical properties and strain-sensing capability of cement-based composites doped with different carbon nanoinclusions, namely MWCNTs, CNFs, CB and GNPs.

While not affecting thermal emittance, that was around 0.87÷0.90 for both plain and composite materials, all carbon nanoinclusions strongly affected the spectral solar reflectance of the materials. In particular, while CNFs, CB and GNPs resulted in an almost uniform diffused solar reflectance of about 15% in the overall solar spectrum wavelength interval, so significantly smaller if compared to the reference cement-based material, MWCNTs determined a much lower decrease in reflectance in the visible and infrared regions and even an increase in reflectance in the ultraviolet range of the test radiation.

GNPs revealed to be the most effective nanoinclusions to increase thermal conductivity and diffusivity, whereby such quantities varied from 0.78 W/mK and 0.52 mm<sup>2</sup>/s, for plain material, to 1.14 W/mK and 0.81 mm<sup>2</sup>/s, for nanocomposite material, respectively. Comparatively smaller increases were instead observed when using different nanoinclusions. This result is conceivably associated to the peculiar structural and geometrical characteristics of GNPs, resulting in a nanostructure with a smaller number of nanoparticles, for a fixed amount of added carbon-based material, that is more apt to distribute the thermal wave, as it was also checked by SEM inspections.

The electrical properties of the materials revealed consistent trends with values of thermal conductivity, whereby the largest increase in electrical conductivity was achieved by using GNPs, ranging from about  $1.7 \cdot 10^{-7}$  ( $\Omega\text{cm}$ )<sup>-1</sup> for the plain material to about  $2.6 \cdot 10^{-6}$  ( $\Omega\text{cm}$ )<sup>-1</sup> for the composite material. The nanoparticles also determined consistent increases in electrical capacitance, which is likely associated to the interface between cement-based matrix and nanoparticles being both resistive and capacitive.

All composites exhibited some piezoresistive properties, that is, the ability to work as strain sensors, outputting measurable variations in electrical resistance under an applied axial deformation. However, MWCNTs significantly outperformed all other nanoparticles, both in terms of gauge factor and in terms of quality of output signals. The same MWCNTs also resulted in a strong increase of the Young modulus of the material, ranging from about 8800 MPa for the plane cement paste to about 23400 MPa for the nanocomposite paste. Other nanofillers did not produce any change in the same Young modulus, which confirms that the shape and aspect ratio of the nanoinclusions play a major role in determining the mechanical properties of the composites and that MWCNTs can be very good nanoreinforcements to enhance mechanical properties of cement-based materials.

Overall, the presented results have confirmed that carbon nanoinclusions provide cement-based materials with a variety of key functional properties, that can be useful in various applications pertaining to smart materials and energy efficiency. However, because of their different aspect ratios, different carbon nanoinclusions are useful for specific purposes. Just as illustrative examples, MWCNTs were seen to be particularly efficient in providing the material with strain-sensing capabilities and in protecting its surface against the damaging UV rays, while GNPs showed ideal to increase thermal and electrical conductivities that could be crucial in applications such as heating pavements, geothermal pile foundations, electromagnetic shielding and more.

### **Acknowledgements**

This research was partially supported by Regione Umbria, within POR Umbria ESF 2007–2013, Axis II "Employability" Objective "e" Axis IV "Human Capital" Objective "I". The first author's acknowledgments are also due to the "CIRIAF program for UNESCO" in the framework of the UNESCO Chair "Water Resources Management and Culture", for supporting her research.

### **References**

- [1] Y. Kang, S.G. Jeong, S. Wi, S. Kim, Energy efficient Bio-based PCM with silica fume composites to apply in concrete for energy saving in buildings, *Sol. Energ. Mat. Sol. Cells* 143 (2015) 430–434.
- [2] F. Ubertini, A.L. Materazzi, A. D'Alessandro, S. Laflamme, Natural frequencies identification of a reinforced concrete beam using carbon nanotube cement-based sensors, *Eng. Struct.* 60 (2014) 265–275.

- [3] Y. Wu, J.Y. Wang, P.J.M. Monteiro, M.H Zhang, Development of ultra-lightweight cement composites with low thermal conductivity and high specific strength for energy efficient buildings, *Constr. Build. Mater.* 87 (2015) 100–112.
- [4] M.S. Anwar, B. Sujitha, R. Vedalakshmi, Light-weight cementitious conductive anode for impressed current cathodic protection of steel reinforced concrete application, *Constr. Build. Mater.* 71(2014) 167–180.
- [5] J. Jeon, S.G. Jeong, J.H. Lee, J. Seo, S. Kim, High thermal performance composite PCMs loading xGnP for application to building using radiant floor heating system, *Sol. Energ. Mat. Sol. Cells* 101 (2012) 51–56.
- [6] F. D'Alessandro, F. Asdrubali, G. Baldinelli, Multi-parametric characterization of a sustainable lightweight concrete containing polymers derived from electric wires, *Constr. Build. Mater.* 68 (2014), 277-284.
- [7] S. Naganathan, C.S.J. Singh, Y.W. Shen, P.E. Kiat, S. Thiruchelvam, Nanotechnology in civil engineering - A review, *Adv. Mat. Res.* 935 (2014) 151–154.
- [8] D. Karamanis, E. Kyritsi, S. Krimpalis, Well-ordered nanoporous materials for low-temperature water phase changes and solar evaporative cooling, *Sol. Energ. Mat. Sol. Cells* 139 (2015) 34–43.
- [9] R. Levinson, H. Akbari, P. Berdahl, K. Wood, W. Skilton, J. Petersheim, A novel technique for the production of cool colored concrete tile and asphalt shingle roofing products, *Sol. Energ. Mat. Sol. Cells* 94 (2010) 946–954.
- [10] A. D'Alessandro, M. Rallini, F. Ubertini, A.L. Materazzi, J.M. Kenny, Investigations on scalable fabrication procedures for self-sensing carbon nanotube cement-matrix composites for SHM applications, *Cement Concrete Comp.* 65 (2016) 200–213.
- [11] C. Barreneche, L. Navarro, A. de Gracia, A. Fernández, L.F. Cabeza, In situ thermal and acoustic performance and environmental impact of the introduction of a shape-stabilized PCM layer for building applications, *Renew. Energ.* 85 (2016) 281–286.
- [12] J. Giro-Paloma, M. Martínez, L.F. Cabeza, A.I. Fernández, Types, methods, techniques, and applications for microencapsulated phase change materials (MPCM): A review, *Renew. Sust. Energ. Rew.* 53 (2016) 1059–1075.

- [13] Y. Han, J.E. Taylor, A.L. Pisello, Toward mitigating urban heat island effects: Investigating the thermal-energy impact of bio-inspired retro-reflective building envelopes in dense urban settings, *Energ. Buildings* 102 (2015) 380–389.
- [14] P. Schossig, H.M. Henning, S. Gschwander, T. Haussmann, Micro-encapsulated phase-change materials integrated into construction materials, *Sol. Energ. Mat. Sol. Cells* 89 (2-3) (2005) 297–306. DOI: 10.1016/j.solmat.2005.01.017.
- [15] R. Nikolić, M. Marinović-Cincović, S. Gadžurić, I.J. Zsigrai, New materials for solar thermal storage - Solid/liquid transitions in fatty acid esters, *Sol. Energ. Mat. Sol. Cells*, 79(3) (2003) 285–292.
- [16] P. Bevilacqua, J. Coma, G. Pérez, C. Chocarro, A. Juárez, C. Solé, M. De Simone, L.F. Cabeza, Plant cover and floristic composition effect on thermal behaviour of extensive green roofs, *Building and Environment* 92 (2015) 305–316.
- [17] Y. Han, J.E. Taylor, A.L. Pisello, Toward mitigating urban heat island effects: Investigating the thermal-energy impact of bio-inspired retro-reflective building envelopes in dense urban settings, *Energ. Buildings* 102 (2015) 380–389.
- [18] T. Karlessi, M. Santamouris, Research on thermochromic and pcm doped infrared reflective coatings, in: D.-D. Kolokotsa, M. Santamouris and H. Akbari (Eds.) *Advances in the Development of Cool Materials for the Built Environment*, Bentham Books (2013) 83–103.
- [19] A.M. Khudhair, M.M. Farid, A review on energy conservation in building applications with thermal storage by latent heat using phase change materials, *Energ. Convers. Manage.* 45 (2) (2004) 263–275.
- [20] M. Pulselli, E. Simoncini, R. Ridolfi, S. Bastianoni, Specific energy of cement and concrete: An energy-based appraisal of building materials and their transport, *Ecol. Indic.* 8(5) (2008) 647–656.
- [21] F. Salata, I. Golasi, A.D.L. Vollaro, R.D.L. Vollaro, How high albedo and traditional buildings' materials and vegetation affect the quality of urban microclimate. A case study, *Energ. Buildings* 99 (2015) 32–44.
- [22] I.Z. Bribián, A.V. Capilla, A.A. Usón, Life cycle assessment of building materials: Comparative analysis of energy and environmental impacts and evaluation of the eco-efficiency improvement potential, *Build. Environ.* 46(5) (2011) 1133–1140.

- [23] A. Cuchí, G. Wadel, F. Lopez, A. Sagra, Guía de la eficiencia energética para los administradores de fincas, Fundación Gas Natural, Barcelona (2007) 10–11.
- [24] M. Jalal, A. Pouladkhan, O.F. Harandi, D. Jafari, Comparative study on effects of Class F fly ash, nano silica and silica fume on properties of high performance self compacting concrete, *Constr. Build. Mater.* 94 (2015) 90–104.
- [25] F. Ubertini, A. D'Alessandro, M. Rallini, S. Laflamme, A.L. Materazzi, J.M. Kenny, Strain-sensing carbon nanotube cement-based composites for applications in structural health monitoring: Preparation and modelling issues, UNCECOMP 2015 – 1st ECCOMAS Thematic Conference on Uncertainty Quantification in Computational Sciences and Engineering, (2015) 488–496.
- [26] I. Kang, Y.Y. Heung, J.H. Kim, J.W. Lee, R. Gollapudi, S. Subramaniam, S. Narasimhadevara, D. Hurd, G.R. Kirikera, V. Shanov, M.J. Schulz, D. Shi, J. Boerio, S. Mall, M. Ruggles-Wren, Introduction to carbon nanotube and nanofiber smart materials, *Compos. Part B-Eng* 37 (2006) 382–394.
- [27] S. Laflamme, F. Ubertini, H. Saleem, A. D'Alessandro, A. Downey, H. Ceylan, A.L. Materazzi, Dynamic Characterization of a Soft Elastomeric Capacitor for Structural Health Monitoring. *J. Struct. Eng.-ASCE* 141(8) (2015).
- [28] F. Sanchez, K. Sobolev, Nanotechnology in concrete – A review, *Constr. Build. Mater.* 24 (2010) 2060–2071.
- [29] D.D.L. Chung, Carbon materials for structural self-sensing, electromagnetic shielding and thermal interfacing, *Carbon* 50 (2012) 3342–3353.
- [30] S-N. Lu, N. Xie, L-C. Feng, J. Zhong, Applications of Nanostructured Carbon Materials in Constructions: The State of the Art, *J. Nanomater.* 2015 (2015) 10 pp.
- [31] F. Azhari, N. Banthia, Cement-based sensors with carbon fibers and carbon nanotubes for piezoresistive sensing, *Cement Concrete Comp.* 34 (2012) 866–873.
- [32] O. Galao, F.J. Baeza, E. Zornoza, P. Garcés, Strain and damage sensing properties on multifunctional cement composites with CNF admixture, *Cement Concrete Comp.* 46 (2014) 90–98.
- [33] B. Han, S. Sun, S. Ding, L. Zhang, X. Yu, J. Ou, Review of nanocarbon-engineered multifunctional cementitious composites, *Compos. Part B-Appl. S.* 70 (2015) 69–81.

- [35] B. Han, S. Ding, X. Yu, Intrinsic self-sensing concrete and structures: A review, *Measurement* 59 (2015) 110–128.
- [36] F. Ubertini, S. Laflamme, H. Ceylan, Halil, A.L. Materazzi, G. Cerni, H. Saleem, A. D'Alessandro, A. Corradini, Novel Nanocomposite Technologies for Dynamic Monitoring of Structures: a Comparison between Embedded and Surface Sensors, *Smart Mater. Struct.* 23(4) (2014) 12pp.
- [37] M.S. Konsta-Gdoutos, C.A. Aza, Self sensing carbon nanotube (CNT) and nanofiber (CNF) cementitious composites for real time damage assessment in smart structures, *Cement Concrete Comp.* 53 (2014) 162–169.
- [38] S. Wen, D.D.L. Chung, Damage monitoring of cement paste by electrical resistance measurement, *Cement Concrete Res.* 30 (2000) 1979–1982.
- [39] J. Gomis, O. Galao, V. Gomis, E. Zornoza, P. Garcés, Self-heating and deicing conductive cement, *Constr. Build. Mater.* 75 (2015) 442–449.
- [40] A. D'Alessandro, F. Ubertini, A.L. Materazzi, S. Laflamme, M. Porfiri, Electromechanical modelling of a new class of nanocomposite cement-based sensors for structural health monitoring, *Struct. Health Monit.* 14 (2) (2015) 137–147.
- [41] Q. Li, J. Liu, S. Xu, Progress in Research on Carbon Nanotubes Reinforced Cementitious Composites, *Adv. Mater. Sci. Eng.* 2015 (2015) 16 pp.
- [42] B. Han, X. Guan, J. Ou, Electrode design, measuring method and data acquisition system of carbon fiber cement paste piezoresistive sensors, *Sensor. Actuat A-Phys* 135 (2007) 360–369.
- [43] M.S. Konsta-Gdoutos, Z.S. Metexa, S.P. Shah, Highly dispersed carbon nanotube reinforced cement-based materials, *Cem. Concr. Res.* 40(7) (2010) 1052–1059.
- [44] F. Ko, Y. Gogotsi, A. Ali, N. Naguib, H. Ye, G.L. Yang, C. Li, P. Willis, Electrospinning of continuous carbon nanotube-filled nanofiber yarns. *Adv. Mater.* 15 (2003) 1161–1165.
- [45] J. Makar, J. Beaudoin, Carbon nanotubes and their application in the construction industry. In: P. Bartos, et al., eds. *Proceedings of the 1st international symposium on nanotechnology in construction NICOM* (2003) 331–341.

[46] S.J. Chen, F.G. Collins, A.J.N. Macleod, Z. R.K. Abu Al-Rub, A.I. Ashour, B.M. Tyson, On the aspect ratio effect of multi-walled carbon nanotube reinforcements on the mechanical properties of cementitious nanocomposites, *Constr. Build. Mater.* 35 (2012) 647–655.

[47] T. Page McAndrew, P. Laurent, M. Havel, C. Roger, Arkema graphistrength® multi-walled carbon nanotubes, Technical Proceedings of the 2008 NSTI Nanotechnology Conference and Trade Show, NSTI-Nanotech, *Nanotechnology* 2008 1 (2008) 47–50.

[48] Carbon nanotube-cement composites: A retrospect, *The IES Journal Part A: Civil & Structural Engineering* 4(4) (2011) 254-265.

[49] J. Sánchez-González, A. Macías-García, M.F. Alexandre-Francob, V. Gómez-Serrano, Electrical conductivity of carbon blacks under compression, *Carbon* 43(4) (2005) 741–747.

[50] J-L. Le, H. Du, S.D. Pang, Use of 2D Graphene Nanoplatelets (GNP) in cement composites for structural health evaluation, *Compos. Part B-Eng* 67 (2014) 555–563.

[51] EN 12667:2001 Thermal performance of building materials and products - Determination of thermal resistance by means of guarded hot plate and heat flow meter methods - Products of high and medium thermal resistance.

[52] EN ISO 22007-2:2012 Plastics - Determination of thermal conductivity and thermal diffusivity - Part 2: Transient plane heat source (hot disc) method (ISO 22007-2:2008).

[53] M. Gustavsson, E. Karawacki, S.E. Gustafsson, Thermal conductivity, thermal diffusivity, and specific heat of thin samples from transient measurements with hot disk sensors, *Rev. Sci. Instrum.* 65 (12) (1994) 3856-3859.

[54] Hot disk thermal constant analyser Instruction Manual 2014.

[55] Standard Test Method for Solar Absorptance, Reflectance, and Transmittance of Materials Using Integrating Spheres; ASTM E903-96; American Society for Testing and Materials: West Conshohocken, PA, USA, 1996.

[56] Standard Test Method for Determination of Emittance of Materials Near Room Temperature Using Portable Emissometers; ASTM C1371-04a; American Society for Testing and Materials: West Conshohocken, PA, USA, 2010.

- [57] Rui Zhang, Guosheng Jiang, and Jia Liang. The Albedo of Pervious Cement Concrete Linearly Decreases with Porosity, *Adv. Mater. Sci. Eng.* 2015 (2015)
- [58] R. Paolini, M. Zinzi, T. Poli, E. Carnielo, A. G. Mainini, Effect of ageing on solar spectral reflectance of roofing membranes: Natural exposure in Roma and Milano and the impact on the energy needs of commercial buildings, *Energ. Buildings* 84 (2014) 333–343.
- [59] F. Pini, C. Ferrari, A. Libbra, F. Leali, A. Muscio, Robotic implementation of the slide method for measurement of the thermal emissivity of building elements, *Energ. Buildings* (2015) in press. doi:10.1016/j.enbuild.2015.07.034.
- [60] M. Fasano, M.B. Bigdeli, M.R. Vaziri Sereshk, E. Chiavazzo, P. Asinari, Thermal transmittance of carbon nanotube networks: Guidelines for novel thermal storage systems and polymeric material of thermal interest, *Renew. Sust. Energ. Rew.* 41 (2015) 1028–1036.
- [61] V.V. Chaban, O.V. Prezhdo, Water Boiling Inside Carbon Nanotubes: Toward Efficient Drug Release, *ACS Nano* 5 (2011) 5647-5655.
- [62] S. Wen, D.D.L. Chung, Effect of stress on the electric polarization in cement, *Cement Concrete Res.* 31 (2001) 291–295.
- [63] B. Chen, K Wu, W. Yao, Conductivity of carbon fiber reinforced cement-based composites, *Cement Concrete Comp.* 26 (2004) 291–297.
- [64] G.Y. Li, P.M. Wang, X. Zhao, Pressure-sensitive properties and microstructure of carbon nanotube reinforced cement composites, *Cement Concrete Comp.* 29 (2007) 377–382.
- [65] P. Xie, P. Gu, J.J. Beaudoin, Electrical percolation phenomena in cement composites containing conductive fibres, *J. Mater. Sci.* 31 (1996) 4093–4097.